Available online at www.sciencedirect.com
ScienceDirect
Journal of Catalysis 246 (2007) 193–204
JOURNAL OF CATALYSIS
www.elsevier.com/locate/jcat

Production of hydrogen by steam reforming of methanol over Cu/ZnO catalysts prepared via a practical soft reactive grinding route based on dry oxalate-precursor synthesis

Lu-Cun Wang, Yong-Mei Liu, Miao Chen, Yong Cao *, He-Yong He, Gui-Sheng Wu, Wei-Lin Dai, Kang-Nian Fan

Department of Chemistry & Shanghai Key Laboratory of Molecular Catalysis and Innovative Materials, Fudan University, Shanghai 200433, PR China

Received 9 October 2006; revised 4 December 2006; accepted 8 December 2006

Available online 10 January 2007

Abstract

Binary Cu/ZnO catalysts (with a Cu/Zn atomic ratio of 50/50) prepared via a novel dry synthetic approach based on solid-state oxalate-precursor synthesis were studied in regard to their performance in the steam reforming of methanol (SRM). The synthesis route involves facile solid-phase mechanochemical activation of a physical mixture of simple copper/zinc salts and oxalic acid, followed by calcination of the as-ground oxalate precursors at 350 °C. For comparison, their conventional analogues obtained by aqueous coprecipitation techniques were also examined. Structural characterization of the samples was performed by means of N_2 adsorption, X-ray diffraction (XRD), diffuse reflectance infrared Fourier transform spectroscopy (DRIFTS), thermal gravimetric and differential thermal analysis (TG/DTA), scanning electron microscopy (SEM), temperature-programmed reduction (H_2-TPR), N_2O titration, and X-ray photoelectron spectroscopy (XPS). The results show that the grinding-derived Cu/ZnO catalysts exhibit superior SRM performance to their conventional counterparts obtained by wet-chemical methods. The enhanced performance of the grinding-derived catalysts can be attributed to a higher copper dispersion as well as the beneficial generation of highly strained Cu nanocrystals in the working catalyst. It is proposed that the present soft reactive grinding route based on dry oxalate-precursor synthesis can allow the generation of a new type of Cu/ZnO materials with favorable surface and structural properties, providing an attractive alternative for preparation of improved heterogeneous catalysts.

Keywords: Steam reforming of methanol; Cu/ZnO catalyst; Dry synthetic approach; Soft reactive grinding; Oxalate precursor

1. Introduction

Catalysts based on copper–zinc mixed oxides are of great importance in industrial catalytic processes like low-pressure methanol synthesis and the water–gas shift reaction [1–8]. It is also established that Cu/ZnO-containing materials are effective catalysts for a number of hydrogenation and dehydrogenation reactions, including oxo-alcohol manufacturing from hydroformylation processes and ketone synthesis by alcohol dehydrogenation [9,10]. Because of its ever-increasing industrial importance, the Cu/ZnO material has become one of the most widely studied systems in heterogeneous catalysis [11]. Nevertheless, despite decades of research, controversy remains regarding the precise nature of the active sites for methanol synthesis or related processes [5,12–15]. The consensus in the literature is that ZnO plays a vital role in obtaining and maintaining the active copper in optimal dispersion [3]. The high activity of this particular system is believed to result from a strong interaction of the two phases leading to a unique activation of the copper species [12–17].

To date, numerous technical methods, including wet-chemical processes, such as alkali solution coprecipitation [2–7,16, 18–21], aqueous impregnation [22], sol–gel processes [23], reverse microemulsion techniques [24,25], as well as various dry-chemical techniques, such as high-energy ball milling [26–28], chemical vapor deposition [29], and flame combustion synthesis [30], have been developed to prepare copper/zinc mixed ox-

* Corresponding author. Fax: +86 21 65642978.
E-mail address: yongcao@fudan.edu.cn (Y. Cao).

0021-9517/$ – see front matter
doi:10.1016/j.jcat.2006.12.006

ide catalysts for various applications. Among these techniques, coprecipitation via hydroxycarbonate (HC) precursors followed by calcination has shown to be practical for commercial production of well-mixed Cu/ZnO-based catalysts [1–7]. However, this ill-defined process often has disadvantages, such as tedious multistep processing and the need for delicate pH/temperature control [1,7]. In addition, the final material obtained from the alkali coprecipitation route suffers from the contamination of alkaline metals as well as the formation of vast amount of environmental wastes (e.g., salts from hydrolysis and washwater). To circumvent these problems, the development of new practical and effective methods for preparation of the Cu/ZnO-based multicomponent catalyst system with a strong copper–zinc interaction is highly desirable.

Over the last two decades, increasing attention has been paid to the steam reforming of methanol (SRM) to produce high-purity hydrogen used in fuel cells for on-board power generation for vehicles [16,17,20,24,31]. Recently, the reformed methanol has been proposed as a useful feedstock for a number of chemical processes [32]. These applications require catalysts with high activity, selectivity, and stability under reaction conditions [16,31]. Numerous Cu/ZnO-based catalysts with various modifications have been tested [16–21]. Our previous studies have shown that mixed copper/zinc oxalates derived from alcoholic or aqueous coprecipitation are well-established sodium-free precursors for the synthesis of highly effective Cu/ZnO-based catalysts for both methanol synthesis from CO_2 hydrogenation and SRM [5,18,33]. It was also shown that these oxalate-derived copper-based catalysts exhibited improved long-term stability during the SRM reaction compared with their conventional HC-precursor derived counterparts [18]. More recently, the combination of the oxalate-precursor coprecipitation procedure with the microemulsion technique for preparing well-mixed Cu/ZnO catalysts was also reported [24,25].

On the other hand, reactive grinding based on mechanochemical activation has long been known as a technique for refining particles of solid materials and promoting mechanical activation of solid-state displacement reactions, which has been successfully applied in the synthesis of various nanostructured metal and metal-oxide phases [26,34–38]. The highly nonequilibratory nature of the grinding process may provide a unique opportunity to prepare catalytic materials with improved and/or novel physical and chemical properties [37,38]. Moreover, reactive grinding can be done easily under solvent-free conditions and rapidly produces large amounts of well-mixed nanocomposites [39]. Recently, it was reported that the binary Cu/ZnO catalysts could be prepared by high-intensity mechanical mixing of metallic copper and zinc oxide powder at ambient conditions, which showed a methanol synthesis activity comparable to conventional Cu/ZnO obtained by HC coprecipitation [26–28]. Despite the great potential practical applications, one notable shortcoming of the above method is that an extended processing time (up to 100 h) is required to obtain a final catalyst with optimal catalytic activities.

In this study, we report the development of a new, simple, waste-free, energy-saving dry-chemical approach based on solid-phase synthesis of oxalate-precursor via a novel soft reactive grinding procedure for the effective preparation of a novel binary Cu/ZnO catalyst that is highly efficient in hydrogen production from SRM. The initial stage of the grinding route involves the facile solid-phase mechanochemical reaction (Scheme 1) of basic carbonates or nitrates of copper/zinc compounds with oxalic acid to yield well-mixed Cu–Zn oxalate precursors at ambient conditions. Special attention is paid to the effects of the copper/zinc precursor salts and the grinding time on their structural properties and catalytic behavior in the SRM process. The structure-activity relationship of the Cu/ZnO materials is evaluated in light of a detailed characterization of the physicochemical properties of the catalysts by N_2 adsorption, XRD, DRIFTS, TG/DTA, SEM, N_2O titration, TPR, and XPS.

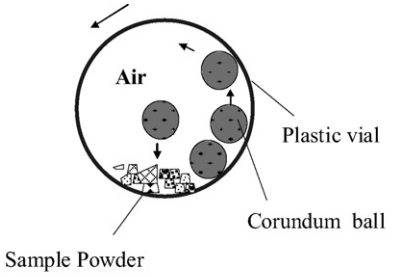

$$M_xCO_3(OH)_{2x-2}(s) + xH_2C_2O_4\cdot 2H_2O(s) \xrightarrow{\text{Grinding}}$$

$$xMC_2O_4(s) + (4x-1)H_2O(l) + CO_2(g) \qquad M = Cu \text{ or } Zn$$

Scheme 1. The soft reactive grinding process based on dry oxalate-precursor synthesis for the preparation of copper–zinc mixed oxide catalysts.

2. Experimental

2.1. Catalyst preparation

Four types of Cu/ZnO samples (all with a Cu/Zn atomic ratio of 50/50) were prepared by different dry- and wet-chemical synthesis methods, including soft reactive grinding of oxalic acid with the Cu/Zn basic carbonate precursors (GC-CZ), soft reactive grinding of oxalic acid with the Cu/Zn nitrate precursors (GN-CZ), aqueous coprecipitation via the hydroxycarbonate precursors (CC-CZ), and aqueous coprecipitation via oxalate precursors (OC-CZ). The synthesis procedures are described in detail below.

A typical procedure for preparing the GC-CZ catalysts is as follows. First, 4.15 g of $Cu_2CO_3(OH)_2$, 4.13 g of $Zn_5(OH)_6(CO_3)_2$, and 10.16 g of $H_2C_2O_4\cdot 2H_2O$ were premixed by hand grinding for ca. 5 min. The mixed powder was then loaded into a plastic vial (50 ml) with corundum milling balls (3–5 mm) under air atmosphere. The weight ratio of the balls and powders was 5:1. The grinding was carried out in a planetary mill (QM-1SP04) at a speed of 560 rpm for 0.5, 2, 4, 8, and 12 h. After the completion of grinding, the as-ground oxalate precursor was separated from the balls, followed by calcination at 350 °C in air for 4 h. The final calcined samples were designated as GC-CZ-*t*, where *t* denotes grinding time (see Table 1).

The procedure for preparing the GN-CZ catalyst was similar to that of GC-CZ, except with nitrates (i.e., $Cu(NO_3)_2{\cdot}3H_2O$ and $Zn(NO_3)_2{\cdot}6H_2O$) replacing carbonates and the grinding time fixed at 4 h.

For comparison, two reference Cu/ZnO catalysts obtained by wet-chemical methods were prepared. The CC-CZ catalyst was prepared by hydroxycarbonate (HC) coprecipitation in aqueous solution as described previously [19]. In brief, a 1.2 M aqueous solution of Na_2CO_3 was added to an aqueous solution of Cu and Zn nitrates (each 0.5 M) under ambient atmosphere and vigorous stirring. During precipitation, the temperature was maintained at 60 °C and pH was kept at 8.5. The precipitates were washed thoroughly and dried in air at 110 °C for 12 h, followed by calcination at 350 °C for 4 h. The OC-CZ catalyst was prepared by oxalate-coprecipitation in an aqueous solution as described previously [18]. Briefly, an aqueous solution of 20% excess of oxalic acid was injected rapidly into a mixed aqueous solution of copper nitrate and zinc nitrate (each 0.1 M) at room temperature under vigorous stirring. The resultant precipitates were dried at 110 °C overnight, followed by calcination at 350 °C for 4 h.

2.2. Catalyst characterization

The BET specific surface areas of the calcined catalysts were determined by adsorption–desorption of nitrogen at liquid nitrogen temperature, using a Micromeritics TriStar 3000 instrument. Sample degassing was carried out at 300 °C before the adsorption isotherm was acquired.

Scanning electron microscopy (SEM) images of the calcined samples were obtained using a Philips XL 30 microscope operating at 30 kV. Before being transferred into the SEM chamber, the samples dispersed with ethanol were deposited on the sample holder and then quickly moved into the vacuum evaporator (LDM-150D).

X-ray powder diffraction (XRD) of the samples was carried out on a Bruker D8 Advance X-ray diffractometer using nickel-filtered Cu$K\alpha$ radiation (1.5406 Å) with a scanning angle (2θ) of 20°–80°, a scanning speed of 2° min^{-1}, a voltage of 40 kV, and a current of 20 mA. The full width at half maximum (FWHM) of (111) reflection of CuO or ZnO was measured for calculating crystallite sizes.

In situ XRD experiments were performed as follows. Reduction of the calcined CuO/ZnO oxide precursors in 5 vol% H_2 in argon from room temperature to 250 °C at a heating ramp of 1 °C min^{-1} was carried out in a Paar XRK-900 high-temperature cell [40]. In situ XRD patterns were recorded at 250 °C under simulated SRM conditions (c(MeOH) ∼ 5 vol%, $c(H_2O)$ ∼ 6.5 vol% in 100 ml min^{-1} Ar) in the 2θ range of 20°–80°, with a step width of 0.02° and a counting time of 1s/dp (dp = data point). XRD patterns of the various Cu/ZnO catalysts under reaction conditions were analyzed by the Pawley method ("full pattern refinement") [12]. The crystallite size corresponding to the broadening of each *hkl* line was determined from the Lorentzian part of the individual profile functions, with the microstrain determined from the Gaussian part [12].

Diffuse reflectance infrared Fourier transform spectroscopy (DRIFTS) characterization of the catalysts was performed using a Bruker Vector 22 spectrometer equipped with a DTGS detector and a KBr beam splitter [41]. The samples were placed in a sample cup inside a Harrick diffuse reflectance cell equipped with ZnSe windows and a thermocouple mount that allowed direct measurement of the sample temperature. All spectra were collected in dry air atmosphere at room temperature.

Thermogravimetric and differential thermal analysis (TG/DTA) measurements were performed on a Perkin–Elmer 7 Series thermal analyzer apparatus in an air flow (30 ml min^{-1}) with a heating rate of 10 °C min^{-1}, using Al_2O_3 as a reference. Between 10 and 15 mg of sample was used for each experiment.

The specific surface area of metallic copper was measured by the adsorption and decomposition of N_2O on the surface of metallic copper as follows: $2Cu_{(s)} + N_2O \rightarrow N_2 + Cu_2O_{(s)}$. The pulse titration technique was used. Pure nitrogen was used as the carrier gas, and a thermal conductivity detector was used to detect the consumption of N_2O [33]. The specific area of metallic copper was calculated from the total amount of N_2O consumption with 1.46×10^{19} copper atoms per m^2 [42].

Temperature-programmed reduction (TPR) profiles were obtained on a homemade apparatus as described previously [18]. Approximately 20 mg of a freshly calcined catalyst was placed on top of glass wool in a quartz reactor. TPR experiments were carried out in 5% H_2/Ar flowing at 40 ml min^{-1}, with a ramp rate of 10 °C min^{-1} to a final temperature of 500 °C. The H_2 consumption was monitored using a TCD.

X-ray photoelectron spectroscopy (XPS) spectra were recorded with a Perkin–Elmer PHI 5000C system equipped with a hemispherical electron energy analyzer. The Mg$K\alpha$ ($h\nu$ = 1253.6 eV) was operated at 15 kV and 20 mA. The carbonaceous C 1s line (284.6 eV) was used as the reference to calibrate the binding energies (BEs). To investigate the nature of Cu species on the surface of the reduced catalysts, XPS characterization after the SRM reaction at 250 °C for 6 h were carried out. The SRM reaction was performed ex situ in a vertical down-flow reactor, similar to that used for the catalytic experiments, after which the samples were cooled to room temperature. The catalysts were retrieved under Ar atmosphere, then quickly measured by XPS.

2.3. Catalytic tests

The catalytic test was conducted using a fixed-bed microreactor from 160 to 300 °C under atmospheric pressure. A 0.5-g catalyst sample diluted with 0.5 g of quartz sand (both in 40–60 mesh) was packed into a stainless steel tubular reactor (6 mm i.d.). After reduction in a H_2/Ar (5/95) flow of 60 ml min^{-1} at 250 °C for 6 h, premixed water and methanol with a H_2O/MeOH molar ratio of 1.3 at a flow rate of 44.0 ml-NTP min^{-1} were fed into the preheater, which was maintained at about 250 °C, using a microfeeder. The vaporized feed entered the reactor with a stream of Ar gas at a flow rate of 20 ml min^{-1} to initiate the SRM reaction at the designated reaction temperature. The reaction products were first passed through a cold trap; then the gaseous products, such as H_2,

Table 1
Physicochemical properties of various Cu/ZnO catalysts prepared by dry oxalate-precursor approach based on soft reactive grinding

Catalyst	S_{BET}[a] ($m^2\,g^{-1}$)	$S_{Cu}^{N_2O}$[b] ($m^2\,g^{-1}$)	S_{Cu}^{XRD}[c] ($m^2\,g^{-1}$)	d_{CuO}[d] (nm)	d_{ZnO}[d] (nm)	d_{Cu}[e] (nm)	d_{ZnO}[e] (nm)	Microstrain[f] (‰)
GC-CZ-0.5	28	3.6	9.3	18.2	12.9	28.4	13.8	1.12
GC-CZ-2	39	7.4	12.2	16.5	11.8	21.7	12.7	1.35
GC-CZ-4	50	11.5	15.0	15.2	11.5	17.6	12.5	2.19
GC-CZ-8	56	19.8	21.0	10.8	9.0	12.6	9.9	2.41
GC-CZ-12	48	12.9	17.7	12.4	11.1	14.9	12.4	2.25
GN-CZ-4	45	14.8	16.4	14.1	10.2	16.1	10.8	2.22
OC-CZ	39	7.8	10.9	17.6	13.1	24.3	14.7	1.69
CC-CZ	34	10.4	13.8	13.2	14.9	19.1	19.2	1.58

[a] BET specific surface area.
[b] Cu metal surface area determined by N_2O decomposition method.
[c] Cu metal surface area estimated by the in situ XRD crystallite size.
[d] d_{CuO} and d_{ZnO} determined by the XRD data of the oxide precursors based on Sherrer equation.
[e] d_{Cu} and d_{ZnO} determined for the working catalyst by the in situ XRD data based on Sherrer equation.
[f] The microstrain of the Cu crystals estimated from the X-ray Cu(111) diffraction lines in working catalysts at 250 °C [14].

CO, CO_2, and CH_4, were detected on-line by a gas chromatograph (type GC-122, Shanghai Analysis) equipped with a TCD and TDX-01 column; the liquid products, such as water and methanol, were analyzed by the same gas chromatograph equipped with another TCD and a Porapak-Q column. Unless specified otherwise, catalytic activity was evaluated from the data collected after 6 h of on-stream operation by methanol conversion (X_{MeOH}), CO_2 selectivity (S_{CO_2}), and CO selectivity (S_{CO}) in the outlet. Catalyst turnover frequencies (TOFs, in s^{-1}) were calculated as the number of hydrogen molecules produced per surface copper atom, as determined by the nitrogen oxide decomposition measurements described above.

3. Results

3.1. Structure of the as-ground oxalate precursors

The XRD patterns of the grinding-derived oxalate precursors prepared by the mechanochemical activation of the basic carbonates of Cu/Zn salts with oxalic acid for different periods of time are shown in Fig. 1. It is evident that the formation of well-defined oxalate phase in the solid starting materials occurs after grinding for only 0.5 h. With prolonged grinding from 2 to 12 h, only two oxalate phases corresponding to $CuC_2O_4{\cdot}xH_2O$ and β-ZnC_2O_4 were identified, further confirming the efficacy of the grinding-assisted solid-state reactions as proposed in Scheme 1. Note that no α-$ZnC_2O_4{\cdot}2H_2O$ phase, which appeared in the conventional oxalate gel-coprecipitation process [5,33], was detected. This suggests that the structure of the oxalate precursors formed by the solvent-free reactive grinding process is markedly different from the oxalate precipitates derived by the conventional wet-chemical method. Also note that the as-ground GC-CZ samples underwent an interesting microstructural evolution during the grinding process. As shown in Fig. 1, the proportion of $CuC_2O_4{\cdot}xH_2O$ with respect to β-ZnC_2O_4 increased appreciably at grinding times exceeding 4 h. This indicates that the grinding-assisted transformation of the starting materials into zinc oxalates occurs preferentially over that for the copper oxalates.

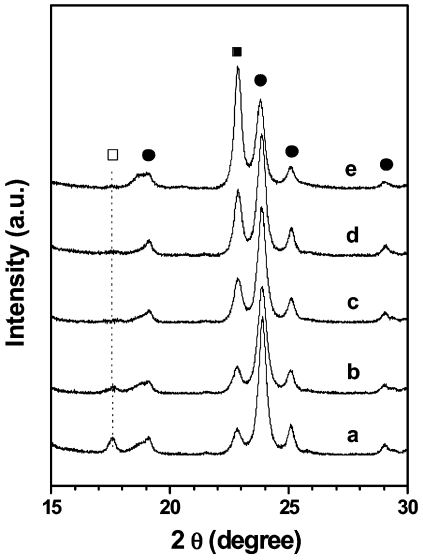

Fig. 1. XRD patterns of the as-ground Cu/Zn mixed oxalate precursors after grinding for different periods of time: (a) GC-CZ-0.5; (b) GC-CZ-2; (c) GC-CZ-4; (d) GC-CZ-8; (e) GC-CZ-12. (■) $CuC_2O_4{\cdot}xH_2O$; (●) β-ZnC_2O_4; (□) $Cu_2CO_3(OH)_2$.

To gain further insight into the reaction kinetics of the grinding process, we followed the formation of the dry Cu–Zn mixed oxalate precursors with FTIR measurements, as shown in Fig. 2. Fig. 2A shows the DRIFTS spectra of the as-ground products after different grinding times. For comparison, the spectra obtained on the three starting materials as well as the reference pure oxalate phases are shown in Fig. 2B. As shown in Fig. 2B, the spectra of the pure copper and zinc basic carbonates display a doublet centered at 1500 cm^{-1} characteristic of the stretching vibrations of CO_3^{2-} moieties [2], in sharp contrast to the spectral features seen for the pure oxalate phases. Comparing the spectrum ground for 0.5 h with that of the reference materials, the peaks from carbonate moieties totally disappears in the ground sample, although the vibration mode of excess amount of pure oxalic acid remains. Moreover, in the spectrum of 0.5 h ground sample, two new bands at 1324 and 1364 cm^{-1}, attributable to symmetric and asymmetric O–C–O

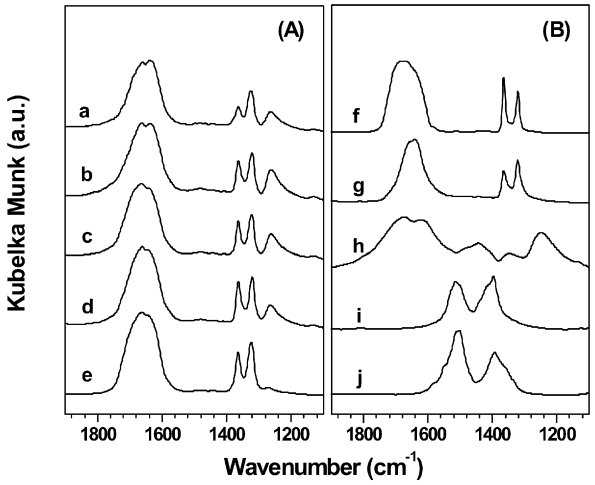

Fig. 2. DRIFT spectra of the as-ground products after grinding for different periods of time: (a) GC-CZ-0.5; (b) GC-CZ-2; (c) GC-CZ-4; (d) GC-CZ-8; (e) GC-CZ-12; (f) $CuC_2O_4{\cdot}xH_2O$; (g) ZnC_2O_4; (h) $H_2C_2O_4{\cdot}2H_2O$; (i) $Cu_2CO_3(OH)_2$; (j) $Zn_5(OH)_6(CO_3)_2$.

stretching modes, respectively, indicative of the formation of well-defined oxalate phases, are clearly shown [43]. With a progressive increase in the grinding time, the resolution and intensity of the oxalate bands increase. This can be ascribed to better crystallinity, in line with the XRD data presented above. Meanwhile, a variation of the peak intensity in the symmetric O–C–O stretching mode with respect to its asymmetric counterpart also can be identified. This may suggest a rearrangement of the oxalate anions in the resulting products [44], inferring a continuous microstructural precursor evolution during the prolonged grinding operation.

Fig. 3 compares the TG/DTA curves of the oxalate precursors (GC-CZ-8) prepared by 8 h of reactive grinding with those of its conventional analogues derived by aqueous oxalate-coprecipitation. Fig. 3B shows that thermal decomposition of the conventional oxalate precipitates at temperatures below 400 °C proceeds via three well-defined steps. The first step starts at about 70 °C, with a broad endothermic DTA peak centered at 92 °C, accompanied by a weight loss of 4.6 wt% attributed for the dehydration of $ZnC_2O_4{\cdot}2H_2O$ and the formation of anhydrous oxalate mixtures [45]. The second step is from 250 to 310 °C, characterized by an exothermic peak at 280 °C showing a weight loss of 17.5 wt%, roughly in accordance with a calculated weight loss of 19.5 wt%, attributed to the decomposition of CuC_2O_4 and formation of the CuO–ZnC_2O_4 mixture [45]. The third step shows an exothermic process with a DTA peak at 340 °C, indicating a weight loss of 26.2 wt% due to further decomposition of ZnC_2O_4 and formation of ZnO. The exothermic character of the DTA peaks accompanying the oxalate decomposition step is due to the air oxidation of CO to CO_2, which commonly occurs in the thermal decomposition of metal oxalate in air [45]. It is interesting that a substantially different thermal evolution behavior was identified for the GC-CZ-8 precursors prepared by the present soft reactive grinding process. As shown in Fig. 3A, a single exotherm related to a one-step thermal decomposition of the two oxalate phases located at 298 °C was observed. These observations un-

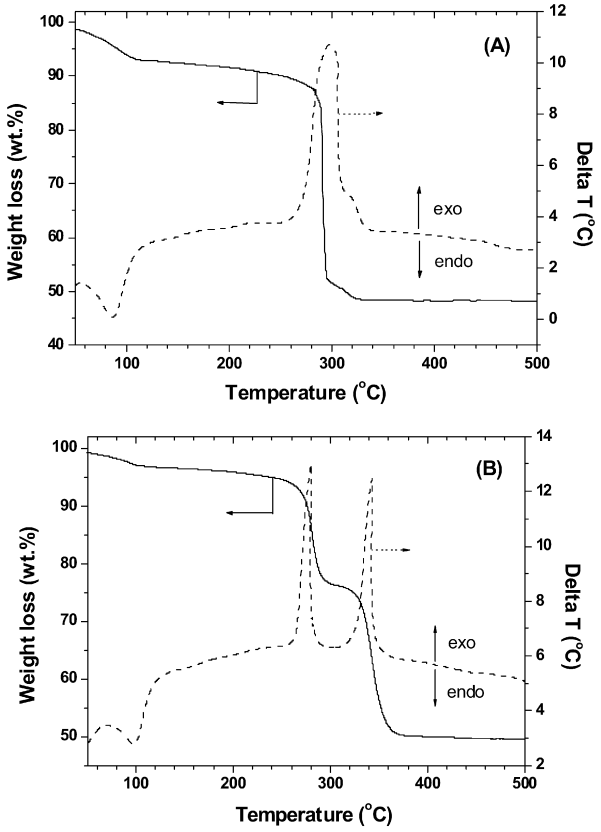

Fig. 3. TG/DTA of the Cu/Zn mixed oxalate precursors prepared by dry- and wet-chemical methods: (A) GC-CZ-8; (B) OC-CZ.

ambiguously reveal that a substantial mechanochemically induced isomorphous substitution between copper and zinc oxalate phases occurs during the grinding process; it has been suggested that this is a key factor in obtaining Cu–Zn mixed oxides with a high component dispersion [5,33].

3.2. Structural and textural features of the calcined catalysts

Fig. 4 shows the surface morphology of the oxide precursors of the grinding-derived Cu/ZnO catalysts along with the samples prepared with two conventional wet-chemical methods. The particles of the grinding-derived catalysts GN-CZ-4 and GC-CZ-4 are sphere-like, and the distribution of the main particles for both samples seems to be practically uniform, with average size <1 μm. In contrast, the samples obtained by conventional coprecipitation methods, especially via the coprecipitation of oxalate precursors, afforded the massive agglomerates apparently much larger than those of the grinding-derived samples. The average particle size is estimated to be about 7 μm for OC-CZ and 3 μm for CC-CZ. Therefore, our SEM results suggest that the soft reactive grinding technique can be more effective than the conventional coprecipitation methods in terms of the preparation of Cu/ZnO catalysts with high component distributions and small particle sizes.

Fig. 5A compares the XRD patterns of calcined catalyst precursors obtained by reactive grinding and the conventional aqueous coprecipitation method using different starting materials. After calcination at 350 °C, all samples are mixtures of CuO

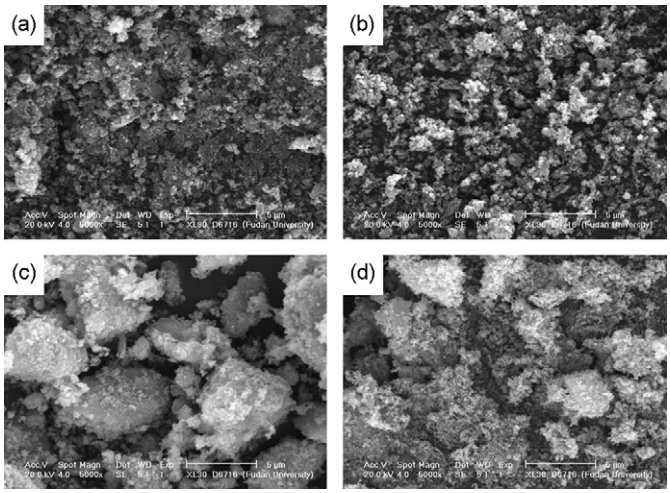

Fig. 4. SEM images of the oxide precursors of the Cu/ZnO samples prepared by various methods: (a) GN-CZ-4; (b) GC-CZ-4; (c) OC-CZ; (d) CC-CZ.

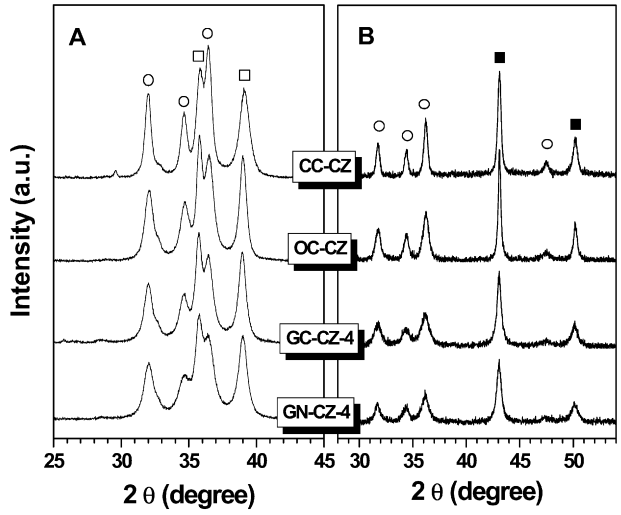

Fig. 5. XRD patterns of the Cu/ZnO catalysts prepared by dry and wet-chemical methods after calcination at 350 °C (A) and followed by reaction at 250 °C (B). (■) Cu phase, (□) CuO phase, (○) ZnO phase.

and ZnO. Comparison of the CuO diffraction lines shows that the CC-CZ sample gives a much broader profile with respect to the other samples, pointing to a weak relationship between the particle size of CuO and the preparation methods. The average crystallite sizes of CuO are estimated using Scherrer's equation and are summarized in Table 1. The CuO crystallite size of CC-CZ was about 13.2 nm; those of OC-CZ, GC-CZ-4 and GN-CZ-4 were somewhat larger, ranging from 14 to 18 nm. It is interesting that average crystallite size as a function of preparation method is significantly different in the ZnO particles. The diffraction lines of the ZnO phases in the grinding-derived Cu/ZnO catalysts are relatively broader and weaker than those of the catalysts prepared by coprecipitation, indicating that the crystallite sizes of ZnO in GN-CZ-4 and GC-CZ-4 are smaller than those in OC-CZ and CC-CZ (see Table 1).

To investigate the active phase of the Cu/ZnO catalysts, the XRD patterns of the four catalysts after reduction followed by subsequent reaction at 250 °C were collected; these are shown in Fig. 5B. Only the metallic copper phase can be seen for all of the samples after reaction. Assuming that Cu particles are spherical, the average copper metal crystallite sizes were calculated from the FWHM of Cu(111) diffraction lines. The results, given in Table 1, reveal much smaller copper particle sizes for GN-CZ-4 (16.1 nm) and GC-CZ-4 (17.6 nm) than compared with OC-CZ (24.3 nm) and CC-CZ (19.1 nm). Note that the copper particle sizes in GN-CZ-4 and GC-CZ-4 were much smaller than that in CC-CZ, in contrast to the relatively larger CuO particle size in the former samples compared with CC-CZ, possibly due to the different Cu–ZnO interaction behavior in these samples [14]. In addition, the grinding-derived Cu/ZnO catalysts can afford the favorable creation of highly strained Cu nanocrystals in the active catalysts. As shown in Table 1, the microstrain values in the copper nanocrystals of GN-CZ-4 and GC-CZ-4 were observed to be much higher than their conventional counterparts, further confirming the presence of a stronger or modified Cu–ZnO interaction in the grinding-derived samples [15,40].

The physicochemical properties of the calcined catalysts prepared by different methods are also presented in Table 1. It is shown that both the BET and active Cu metal surface area of the catalysts prepared by the grinding route are larger than those of the catalysts obtained by conventional coprecipitation. Comparison of the grinding-derived samples using different precursor salts reveals that the catalyst GN-CZ-4 prepared using nitrates as starting materials has a larger BET and Cu metal surface area than GC-CZ-4 derived from carbonate precursors. Note that the specific copper surface areas for the present binary Cu/ZnO catalysts are much smaller than those of ternary $Cu/ZnO/Al_2O_3$ catalysts [6,40], but are very close to the binary Cu/ZnO materials, as reported by Alejo et al. [19]. The data of the metallic Cu surface area in Table 1 clearly demonstrate that the copper dispersion is much higher in the grinding-derived catalyst than in catalysts prepared by conventional wet-chemical methods. Using a quasi-sphere model, we also estimated the copper metal surface area by the crystallite size as determined by the in situ XRD results. For all catalysts, the S_{Cu}^{XRD} values, estimated by XRD measurements, are higher than the $S_{Cu}^{N_2O}$ values. These discrepancies may be due to interactions of the copper particles with ZnO or to deviations from a spherical morphology.

To gain insight into the effect of grinding time on the physicochemical properties of the grinding-derived catalysts, the structural evolution of the GC-CZ catalysts obtained with various grinding time was followed by XRD. The XRD patterns of the catalyst precursor and the in situ XRD patterns under the reaction conditions are shown in Figs. 6A and 6B, respectively. Clearly, the diffraction peaks of CuO and ZnO in the precursors become weaker and broader with an increase in grinding time from 0.5 to 8 h, indicating a continuous decrease in the crystallite sizes for both species. Further grinding of the samples with an extended time of 12 h, however, results in an unexpected crystallite growth in the CuO and ZnO particles, possible due to a nonequilibrium nature of the grinding process [39]. Furthermore, the same trend can be observed for the working catalysts under reaction conditions. The particle sizes of Cu, CuO, and ZnO determined from the respective diffraction peaks in the

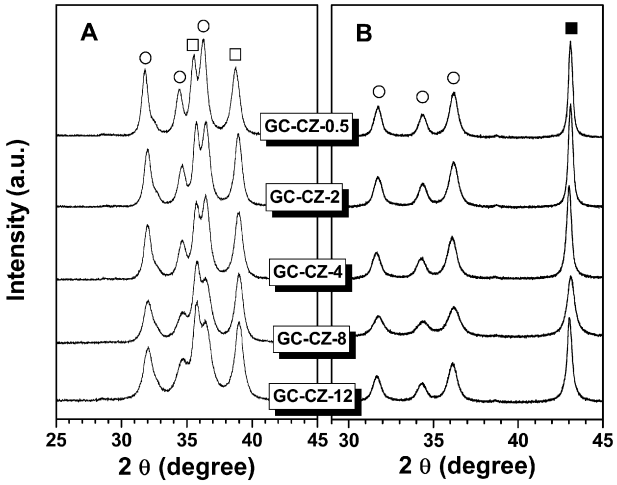

Fig. 6. XRD patterns of the grinding-derived Cu/ZnO catalysts prepared by various grinding time after calcination at 350 °C (A) and followed by reaction at 250 °C (B). (■) Cu phase, (□) CuO phase, (○) ZnO phase.

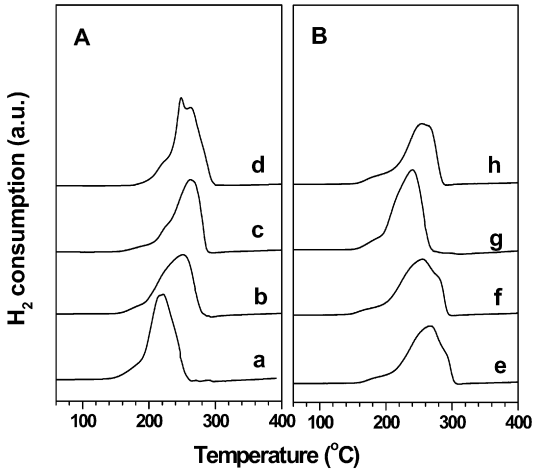

Fig. 7. TPR profiles of the CuO/ZnO catalysts prepared by different methods (A): (a) GN-CZ-4; (b) GC-CZ-4; (c) OC-CZ; (d) CC-CZ and the GC-CZ catalysts with various grinding time (B): (e) GC-CZ-0.5; (f) GC-CZ-2; (g) GC-CZ-8; (h) GC-CZ-12.

XRD patterns are summarized in Table 1. Note that a similar variation trend is also observed for the microstrain values of the copper nanocrystals in the working catalysts.

3.3. Redox properties and chemical states

TPR results were obtained for each of the calcined catalysts. The reduction profiles of the CuO/ZnO catalysts prepared by various methods are shown in Fig. 7. All of the profiles show one main reduction peak, presumably due to the reduction of crystalline CuO, with a shoulder to the main peak identifiable at a lower temperature. This shoulder may be due to the reduction of amorphous or highly dispersed copper oxide species [13]. The GN-CZ-4 catalyst displays the lowest reduction peak at 220 °C, 30 °C lower than that for the GC-CZ-4 catalyst. The CC-CZ sample has a reduction peak at 253 °C, and the OC-CZ sample required a higher temperature of 262 °C to attain a maximum copper oxide reduction rate. The fact that pure bulk

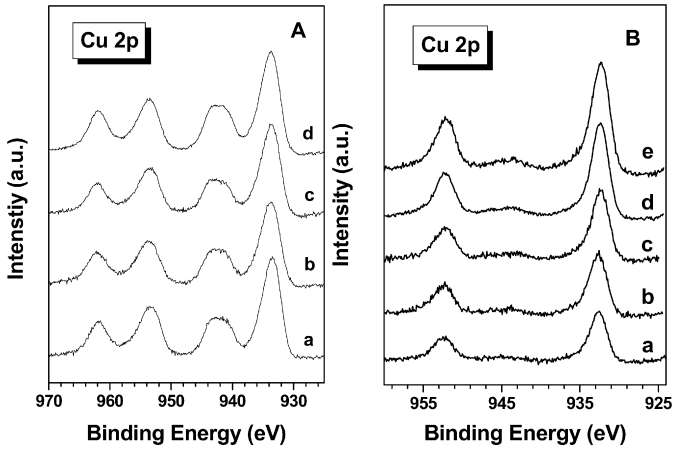

Fig. 8. Cu 2p photoelectron spectra of (A) the calcined CuO/ZnO catalysts prepared by various methods. (a) GN-CZ-4; (b) GC-CZ-4; (c) OC-CZ; (d) CC-CZ; (B) the GC-CZ catalysts obtained with various grinding time after reaction at 250 °C for 6 h. (a) GC-CZ-0.5; (b) GC-CZ-2; (c) GC-CZ-4; (d) GC-CZ-8; (e) GC-CZ-12.

copper oxide is reduced at a considerably higher temperature (ca. 340 °C, not shown) indicates the presence of a copper-support interaction in the present binary samples, which facilitates the reduction of copper oxide. Both bulk and supported CuO are reduced by a process involving nucleation or autocatalytic reduction, and it is well documented that supported CuO can be reduced more readily than bulk CuO [24]. In this situation, it is interesting to note that among the GC-CZ series catalysts (Fig. 7B), the GC-CZ-8 material has the lowest reduction temperature. This indicates that both the precursor salts and grinding time are important parameters in optimizing the redox properties of the grinding-derived catalysts.

On the other hand, it should be noted that GC-CZ-8 displays the lowest reduction temperature of all of the catalysts but GN-CZ-4. This indicates the presence of small CuO or Cu particles and thus a high component dispersion. These results correlate well with the metallic copper surface area measurements, which revealed the highest dispersion in GC-CZ-8. Likewise, there is also good correlation with the XRD measurements showing small CuO and Cu particle sizes in this material. In addition, the reduction profile is narrow and almost symmetrical, indicating a narrow particle size distribution and homogeneous material.

At this point, it should be noted that the TPR findings cannot be explained solely in terms of copper dispersion [5,24]. Indeed, closer comparison of the TPR results with the XRD and N_2O chemisorption measurements reveals that in addition to dispersion, other factors, such as CuO crystallinity and the interaction between the copper and the oxide support, may influence the reducibility of the catalytic materials.

XPS spectra were obtained for the Cu/ZnO samples prepared by various methods and different grinding times to provide information on the chemical states of the copper species on the catalyst surfaces. Fig. 8 shows the Cu 2p spectra of the CZ catalysts after calcination obtained by different methods, along with the spectra recorded for various GC-CZ catalysts after exposure to the reaction conditions. The detailed XPS parameters of all samples are summarized in Table 2. For the calcined catalysts

Table 2
XPS results of various Cu/ZnO catalysts prepared by dry oxalate-precursor approach based on soft reactive grinding

Catalyst	Conditions	BE of Cu $2p_{3/2}$ (eV)[a]	BE of Zn $2p_{3/2}$ (eV)	KE of CuLMM (eV)	α_{Cu} (eV)	Cu/Zn
GC-CZ-0.5	Fresh	933.6 (3.5)	1022.4 (2.6)	917.5	1851.1	0.22
	After reaction	932.6 (2.6)	1022.1 (2.5)	916.8	1849.4	0.12
GC-CZ-2	Fresh	933.5 (3.6)	1022.0 (2.6)	917.8	1851.3	0.28
	After reaction	932.6 (2.7)	1022.0 (2.7)	916.6	1849.2	0.20
GC-CZ-4	Fresh	934.0 (3.7)	1022.5 (2.7)	917.3	1851.3	0.40
	After reaction	932.3 (2.6)	1021.6 (2.7)	917.0	1849.3	0.32
GC-CZ-8	Fresh	933.9 (3.6)	1022.4 (2.7)	917.5	1851.4	0.58
	After reaction	932.3 (2.7)	1021.7 (2.8)	916.7	1849.0	0.48
GC-CZ-12	Fresh	933.7 (3.7)	1021.9 (2.7)	918.2	1851.9	0.46
	After reaction	932.3 (2.6)	1021.8 (2.6)	916.6	1848.9	0.28
GN-CZ-4	Fresh	933.4 (3.6)	1021.9 (2.7)	917.7	1851.2	0.58
	After reaction	932.8 (3.3)	1021.9 (3.2)	916.7	1849.5	0.46
OC-CZ	Fresh	933.6 (3.6)	1022.2 (2.6)	917.7	1851.3	0.48
	After reaction	932.5 (2.6)	1022.2 (2.7)	917.3	1849.8	0.27
CC-CZ	Fresh	933.7 (3.7)	1021.8 (2.7)	917.7	1851.4	0.83
	After reaction	932.7 (2.9)	1021.9 (2.9)	917.0	1849.8	0.42

[a] The values in the parenthesis are FWHM of corresponding main photoemission peaks.

(Fig. 8A), main Cu $2p_{3/2}$ and Cu $2p_{1/2}$ peaks in the BE ranges of 933–934 and 953–954 eV, respectively, with a spin-orbit coupling energy gap of ca. 20 eV, can be seen. Both of these peaks are accompanied by intense satellite features at 942 and 962 eV for all samples. Additional information concerning the precise chemical states of Cu can be obtained from the Auger analysis [46]. As shown in Table 2, the modified Auger parameters α_{Cu} ($\alpha_{Cu} = h\nu + (\mathrm{KE}(\mathrm{Cu_{LMM}}) - \mathrm{KE}(\mathrm{Cu}\ 2p_{3/2}))$) was range of 1851–1852 eV. All of these features are all characteristic of the CuO phase [17,19,47], in line with the XRD results.

After exposure to reaction conditions, the satellite peaks disappeared, accompanied by a shift to lower BEs, ranging from 932.3 to 932.8 eV. This clearly indicates the formation of metallic copper or Cu^+ species [17,19,46]. Because the BEs of Cu^0 and Cu^+ species typically overlap in Cu 2p XPS analysis, these two species can be distinguished only by their different kinetic energies in the Auger Cu_{LMM} line position or the modified Auger parameters α_{Cu} [46]. As shown in Table 2, the Auger parameter of copper varied from 1848.9 to 1849.8 eV, pointing to the presence of Cu^+ species along with the metallic copper [46]. It follows that this result is not in line with our in situ XRD data, which show the exclusive existence of metallic copper in the bulk phase. In fact, the presence of Cu^+ species in the Cu/ZnO samples after exposure to SRM reaction conditions was previously identified by Agrell et al. [47]. Numerous studies have also reported that mildly oxidized copper species may coexist with metallic copper on the surface of the catalysts under working conditions [13,48–53]. However, it is difficult to draw firm conclusions based only on the spectral appearance of Cu^+, because the catalyst surface may be oxidized during cooling after reaction and be further affected by degassing in the XPS pretreatment chamber.

Table 2 also lists the surface atomic ratios of Cu/Zn in various catalysts after different surface pretreatments as measured by XPS. As shown, the surface composition is strongly affected by the preparation methods and grinding time. For all calcined samples, the surface Cu/Zn molar ratio is smaller than that of the bulk phase (i.e., Cu/Zn = 1). Interestingly, the maximum surface Cu/Zn ratio is seen on the catalyst obtained by 8 h of grinding, in line with the variation observed in copper metal surface area as a function of grinding time. After exposure to reaction conditions for 6 h, the surface Cu/Zn ratio decreased in all catalysts, indicating a surface enrichment of Zn species during the initial stages of the SRM reaction. The variation in surface composition for the catalysts before and after reaction also may shed some light onto the stability of various catalysts obtained by different methods and at different milling times. Note that the surface Cu/Zn ratio of the GC-CZ-8 catalyst decreased from 0.58 to 0.48 on exposure to the reaction conditions, whereas those of the catalysts prepared by conventional coprecipitation decreased by nearly half after being subjected to the SRM reaction. This indicates that the catalysts obtained by the reactive grinding technique are superior in maintaining the surface structure of the Cu/ZnO catalysts and thus the catalytic activity for SRM. As for the GC-CZ catalysts prepared with various grinding times, the surface composition of the samples undergoing prolonged grinding appears to be less affected by the reaction conditions, indicating improved stability of the surface structure.

3.4. Catalytic SRM

Fig. 9 shows a typical set of results for SRM over the GC-CZ-8 catalyst, illustrating the effect of temperature on the methanol conversion and the molar compositions with respect to carbon dioxide, hydrogen, and carbon monoxide. As shown, methanol conversion exhibits a typical S-shaped temperature dependence [16,24]. H_2 and CO_2 are produced in an approximate 3:1 ratio, and substantial CO formation is initiated at around 280 °C, when conversion of methanol approaches completeness. Further experiments from our laboratory, as reported previously [18], indicated that CO is not formed at short con-

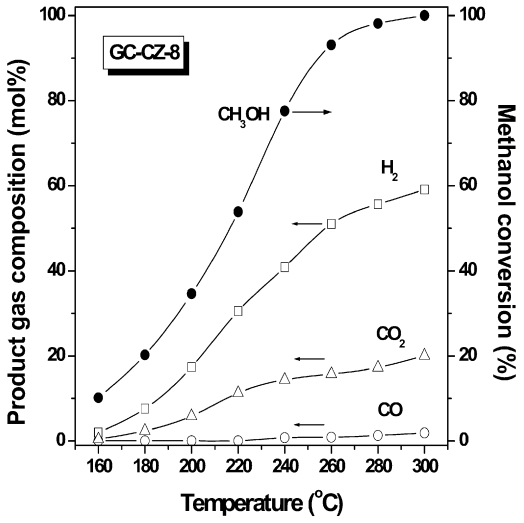

Fig. 9. Product gas composition and methanol conversion vs reaction temperature during steam reforming of methanol over catalyst GC-CZ-8. Conditions—CH_3OH: 19.0 cm^3 min^{-1}; H_2O: 25.0 cm^3 min^{-1}, Ar: 20.0 cm^3 min^{-1}; $H_2O/CH_3OH = 1.3/1$, $p = 0.1$ MPa.

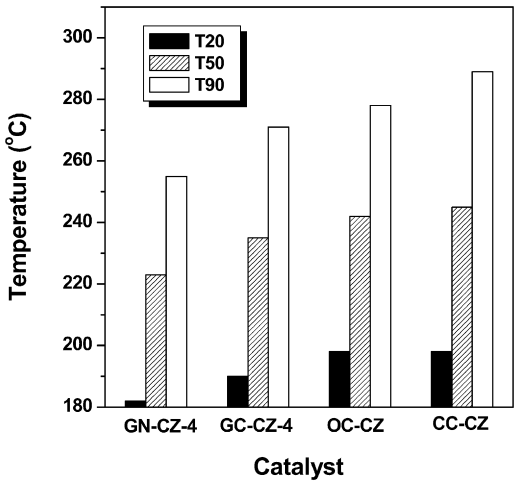

Fig. 10. The temperature required for 20, 50, and 90% conversion of methanol (T_{20}, T_{50}, and T_{90}) during steam reforming over catalysts GN-CZ-4, GC-CZ-4, OC-CZ, and CC-CZ.

tact times and that its concentration becomes significant only when the methanol is almost completely consumed at longer contact times. Moreover, as demonstrated previously [18], the temperature at which complete conversion is achieved can be significantly lowered by decreasing the space velocity. However, optimization with respect to this parameter was not the objective of the present study.

Table 3 summarizes the methanol conversion, selectivity to hydrogen, CO level in the product gas, hydrogen production rates, and turnover frequencies (TOFs) for the SRM over various catalysts. Note that the activity data shown in Table 3 were obtained after 6 h of on-stream reaction, at which point the product composition was found to be stable. The temperature chosen for the comparisons was 240 °C, because, as shown in Fig. 10, the conversion of methanol was well below 100% at this temperature. The selectivities to hydrogen and carbon dioxide were nearly 100% for most of the catalysts. The methanol conversion and hydrogen-production rates from the grinding-derived samples with grinding times longer than 4 h were much higher than those from the conventional wet-chemical-derived samples, possibly due to the much higher copper specific surface area of the former. In particular, the GC-CZ-8 catalyst exhibited the best performance in terms of hydrogen production rate. It is remarkable that the methanol conversion of 78.8% could be achieved over the GC-CZ-8 sample at 240 °C, compared with only ca. 43% over CC-CZ and 48% over OC-CZ.

It is also interesting to further compare the SRM activities for the four catalysts prepared by different methods or processed with the same grinding time. Note that all four catalysts show similar behavior, with the major differences being the temperature at which complete conversion is reached and the level of CO in the reformed gas. The temperatures required to reach 20, 50, and 90% methanol conversion (T_{20}, T_{50}, and T_{90}) over all four catalysts are given in Fig. 10. As shown, the temperatures are consistently lower for the materials prepared by the dry approach based on the soft reactive grinding synthesis. In particular, GN-CZ-4 is very efficient in the SRM reaction, due to a higher copper dispersion and a stronger metal–support interaction. The corresponding CO levels at T_{20}, T_{50}, and T_{90} are shown in Fig. 11, demonstrating that a significant reduction in the CO production could be achieved over grinding-derived Cu/ZnO catalysts.

Table 3
Activity and selectivity for steam reforming of methanol over Cu/ZnO catalysts prepared by different methods[a]

Catalyst[b]	MeOH conversion (%)	Selectivity to hydrogen (%)	CO-level in product gas (%)	H_2 production rate at 240 °C (mmol g_{cat}^{-1} h^{-1})	TOF[c] at 240 °C (10^3 s^{-1})
GC-CZ-0.5	34.0	99.5	0.10	103	328
GC-CZ-2	41.8	99.4	0.12	127	197
GC-CZ-4	52.0	99.2	0.16	158	157
GC-CZ-8	78.8	98.9	0.22	238	138
GC-CZ-12	57.6	99.0	0.20	174	154
GN-CZ-4	70.9	98.7	0.26	214	166
OC-CZ	48.6	98.9	0.22	147	216
CC-CZ	43.0	99.1	0.18	130	143

[a] Reaction conditions—CH_3OH: 19.0 cm^3–NTP min^{-1}; H_2O: 25.0 cm^3–NTP min^{-1}, Ar: 20.0 cm^3 min^{-1}; $H_2O/CH_3OH = 1.3/1$, $p = 0.1$ MPa.
[b] GC: soft reactive grinding synthesis via carbonate precursors; GN: soft reactive grinding synthesis via nitrate precursors, both after grinding for 4 h; OC: coprecipitation via oxalate precursors; CC: coprecipitation via hydroxycarbonate precursors.
[c] Hydrogen molecules produced per surface Cu atom per second.

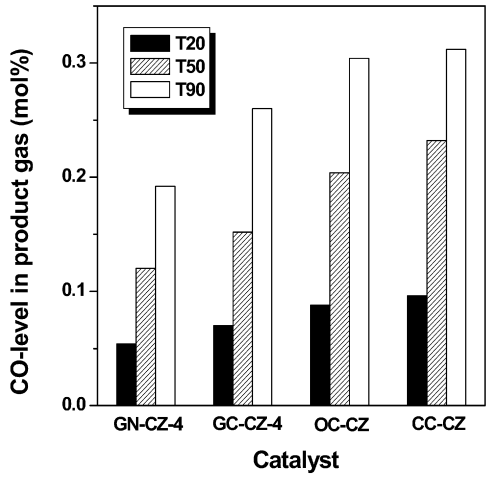

Fig. 11. The CO level in the product gas at 20, 50, and 90% methanol conversion during steam reforming of methanol over catalysts GN-CZ-4, GC-CZ-4, OC-CZ, and CC-CZ.

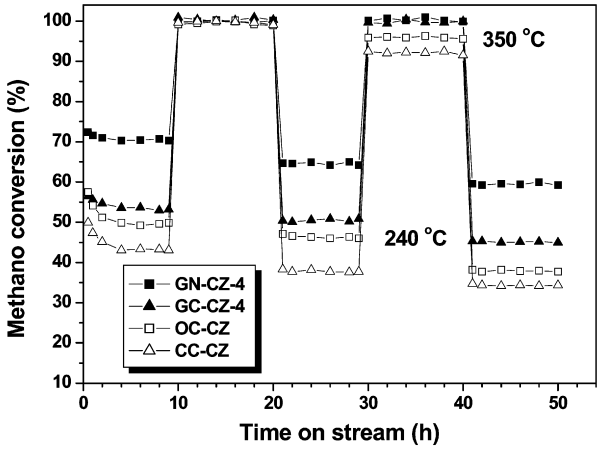

Fig. 12. Influence of accelerated ageing on the methanol conversion rates of catalysts for the steam reforming of methanol. Conditions—CH_3OH: 19.0 $cm^3\,min^{-1}$; H_2O: 25.0 $cm^3\,min^{-1}$, Ar: 20.0 $cm^3\,min^{-1}$; $H_2O/CH_3OH = 1.3/1$, $p = 0.1$ MPa.

To examine the likely long-term behavior of the various catalysts under reaction conditions, an accelerated aging process (i.e., cycling the reactor temperature between 240 and 350 °C) was carried out on the GN-CZ-4, GC-CZ-4, OC-CZ, and CC-CZ catalysts. As shown in Fig. 12, the grinding-derived catalysts were more active and more stable than their conventional counterparts. Comparing the ability of the GN-CZ-4 and GC-CZ-4 catalysts to withstand the effects of aging at 350 °C clearly shows that the GC-CZ-4 catalyst deactivated to a lesser extent than the GN-CZ-4 sample. The GC-CZ-4 catalyst deactivated from an initial steady conversion value of methanol of 52% at 240 °C to 45% after two cycles at 350 °C, corresponding to an activity loss of 14%. This loss of activity compares favorably with that for GN-CZ-4 (i.e., 17%, from an initial steady conversion of 70.9 to 59% after completion of the cycling process). Compared with the grinding-derived catalyst, CC-CZ exhibits relatively poor aging properties despite being more stable than OC-CZ, which deactivated noticeably even during the initial 6 h on stream. Note that both the OC-CZ and CC-CZ catalysts did not give full conversion of methanol at 350 °C during the second cycle. The steady methanol conversion given by the CC-CZ catalyst was 43% initially and declined to 34% after two temperature cycles, corresponding to a decrease of 21%.

4. Discussion

Mechanochemical processing has attracted much attention as a novel and efficient method for producing nanosized materials without severe agglomeration [34–39]. Recently, a wide variety of nanostructured single-oxide or mixed-oxide-based catalyst systems have been synthesized by mechanochemical processing [54–56]. It should be stressed, however, that the solid-state displacement reactions involved in the present soft reactive grinding approach is essentially different from the traditional mechanically activated solid-state reaction between metal–metal oxides, where high temperature or ultra-high-energy intensity, as well as very long processing times, are usually necessary for obtaining a satisfactory product with optimized properties [38,39].

The present work unambiguously demonstrates that the new process, involving the solid-state displacement reaction of oxalic acid with copper and zinc salts induced by planetary ball milling for only several hours, followed by subsequent thermal decomposition, can allow the efficient fabrication of new effective Cu/ZnO catalyst systems with greater surface areas and improved copper dispersion with respect to those of conventional catalysts. The most apparent advantage of the present solvent-free technology is that it avoids excessive energy consumption, long preparation times, and tedious multistep processing, thus providing a new, attractive alternative for preparing well-mixed binary Cu/ZnO catalyst systems.

The grinding kinetics followed by XRD and DRIFTS reveal that the formation of both well-defined copper and zinc oxalate phases in the solid phase occurs after 0.5 h. With prolonged mechanochemical activation, the spectral evolution of both XRD and IR data further demonstrates that the transformation of the starting materials into zinc oxalates is kinetically preferred over that for copper species, especially at the initial stage of the grinding process. With extended precursor grinding, a substantial isomorphous substitution between the copper and zinc oxalates may occur, which is of both theoretical and practical interest for preparing mixed oxide catalysts with higher component dispersion and stronger metal–support interaction. It is noteworthy that the catalyst obtained after 8 h of grinding demonstrates the best performance of all samples, suggesting an optimal copper dispersion or copper–zinc interaction achievable in the active GC-CZ-8 catalyst. It is also noteworthy that nitrates appear to be more effective than carbonates as starting materials, as reflected in the much higher catalytic activity of GN-CZ-4 compared with GC-CZ-4. The formation of environmentally hazardous HNO_3 as a result of precursor grinding makes the use of nitrates as raw materials much less attractive, however.

Meanwhile, investigation by TPR, XRD, and N_2O titration confirms that the thermal decomposition of grinding-derived oxalate precursors leads to greater copper dispersion

and stronger metal–support interactions in the oxide precursors, and thus to improved SRM activity. In situ XRD measurements of the activated catalyst under simulated reaction conditions identified very small or highly strained Cu particles as the main copper phase. The XPS results demonstrate that the surface composition of the present Cu/ZnO catalysts prepared by both the reactive grinding and conventional coprecipitation methods deviated significantly from the bulk composition. The Cu/Zn ratio of calcined and used samples of GC-CZ-8 remained more or less in the same range and showed a correlation with the observed activity and stability. A substantial decrease in the Cu/Zn ratio of the surface and subsurface of SRM catalysts during deactivation for the other seven samples suggests that an optimal surface Cu/Zn ratio around ca. 0.50 is required to obtain high activity and stability. Similar results were obtained by Kumari et al. [57] when correlating the activity and stability of $Cu/ZnO/Al_2O_3$ SRM catalysts with the surface Cu/Zn ratio obtained by SEM-EDAX analysis.

With regard to the essential nature of active copper phase for methanol synthesis or the SRM reaction, the metallic copper surface area generally has been assumed to be the main factor in the structure-activity correlation of Cu-based catalysts [2–7, 18–20]. But some recent studies have found no correlation between the rate of methanol formation or hydrogen production with the surface area of metallic copper for Cu-based catalysts [15,40,58]. Recently, while investigating the effect of continuous precipitate aging on the catalytic performance of a series of hydroxycarbonate-derived Cu/ZnO catalysts, Kniep et al. found that the increased microstrain in the nanostructured Cu particles as detected by XRD and XAS shows an excellent linear correlation with the improved activity of Cu/ZnO in the SRM reaction, as opposed to the variation behavior of the Cu surface area [7,15]. The strain in the supported copper nanoparticles has been suggested to originate from an epitaxial orientation of Cu and ZnO, lattice imperfections caused by Zn incorporated into Cu, or an incomplete reduction of copper [7,14,15]. At this juncture, it is interesting to point out that the extended grinding in the present work is somewhat similar to the aging process in the conventional coprecipitation process. Therefore, it is reasonable to expect that similar conclusions may be drawn as to the effect of grinding time on the microstructural properties and catalytic performance of Cu/ZnO catalysts in the SRM reaction.

To gain further insight into the nature of the copper in the present grinding-derived Cu/ZnO catalysts in relation to SRM activity, the effect of grinding time on the hydrogen production rate as well as the specific copper surface area as determined by surface titration with N_2O is illustrated in Fig. 13. The variation in copper specific surface area shows an excellent correlation with the corresponding hydrogen production rate, and a positive correlation also can be seen between the activity and the lattice microstrain in the copper nanoparticles. This indicates that both Cu surface area and structural disorder contribute to the catalytic activity of Cu/ZnO in the SRM reaction, permitting a rational explanation for the positive grinding effect of precursor processing on active catalyst [14,15]. The lack of a less straightforward correlation between the structural disorder in the copper nanoparticles and the activity in the present case may

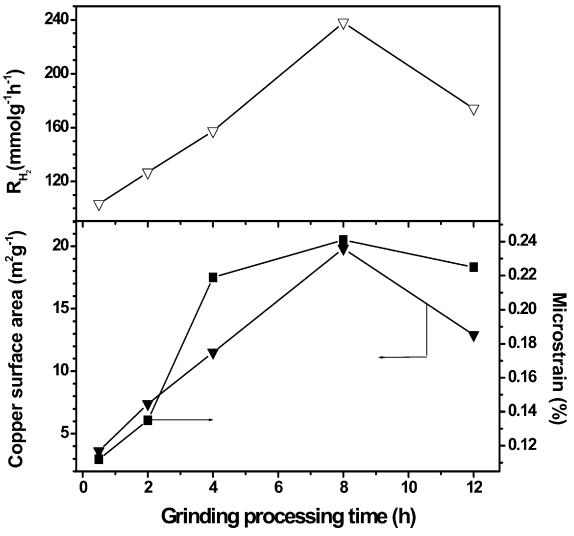

Fig. 13. Hydrogen-production rate R_{H_2} (mmol g_{cat}^{-1} h^{-1}), specific copper surface area measured by N_2O titration (▼) and microstrain (■) of the copper nanoparticles (calculated from Cu(111) line measured at 240 °C) in the GC-CZ catalysts as a function of grinding time on the corresponding oxalate precursors.

be understood by keeping in mind that along with the Cu surface area and structural disorder, other factors, such as interface properties, affect the SRM performance of the grinding-derived Cu/ZnO materials.

Although the main purpose of this paper was to present a novel method for preparing Cu/ZnO catalysts with high copper dispersion and enhanced copper–zinc interaction, here we discuss the possible mechanisms that may explain the grinding process. In the conventional milling process, the central event is the continuous microscopic deformation induced by prolonged mechanochemical activation [30]. Despite intensive grinding, an undesirable equilibrium mixture is obtained in most cases. Under our soft grinding conditions, complete transformation of starting materials into target products can be achieved within several hours. This facile formation of the mixed copper–zinc oxalates is probably due to the use of hydrated compounds as starting materials [39]. In our opinion, this is due to the fact that the presence of crystallization water may facilitate the conversion of activated substances into a plastic state or the generation of a liquid phase via the formation of a liquid layer around the particles. This leads to a substantial increase in the number and overall area of contacts between reactants, thus accelerating component diffusion and creating new conditions for chemical interactions. Moreover, the evolved carbon dioxide (see Scheme 1) also plays an important role in shifting the solid-state reaction to completion. All of these factors result in the facile formation of well-mixed Cu–Zn oxalate precursors at the molecular level during grinding. These findings form the basis for the creation of the new method for synthesizing mixed-oxide catalysts.

5. Conclusions

This study demonstrates that the soft reactive grinding process based on dry oxalate-precursor synthesis provides a new, attractive method for the environmentally friendly and

energy-efficient fabrication of new, improved Cu/ZnO catalysts that are highly effective in the SRM. The superior catalytic performance of the present grinding-derived Cu/ZnO catalyst compared with the wet-chemical-synthesized catalysts obtained by conventional coprecipitation methods can be attributed to greater copper dispersion and the beneficial formation of highly strained copper nanocrystals due to an enhanced copper–zinc interaction in the active working catalyst. By controlling such parameters as the grinding time during the mechanochemical activation process, the dispersion of copper species and the metal–support interaction between copper and zinc oxide can be effectively enhanced, further improving the catalyst's performance in the SRM. Owing to the simplicity and generalizability of the approach used, the present synthetic methodology may be practically extended to the facile and convenient synthesis of other important multicomponent catalyst systems based on well-mixed oxide materials.

Acknowledgments

This work was supported by the National Natural Science Foundation of China (grants 20421303, 20473021, 20633030, and 20503005), the National Basic Research Program of China (grant 2003CB615807), the National High Technology Research and Development Program of China (grant 20060103Z3019), and the Research Fund for the Doctoral Program of Higher Education (grant 20050246071).

References

[1] G. Ertl, H. Knöezinger, J. Weitkamp (Eds.), Handbook of Heterogeneous Catalysis, Wiley–VCH, Weinheim, 1997.
[2] B. Bems, M. Schur, A. Dassenoy, H. Junkes, D. Herein, R. Schlögl, Chem. Eur. J. 9 (2003) 2039.
[3] M.S. Spencer, Top. Catal. 8 (1999) 259.
[4] S.-I. Fujita, S. Moribe, Y. Kanamori, M. Kakudate, N. Takezawa, Appl. Catal. A 207 (2001) 121.
[5] Q. Sun, Y.L. Zhang, H.Y. Chen, J.F. Deng, D. Wu, S.Y. Chen, J. Catal. 167 (1997) 92.
[6] B.A. Peppley, J.C. Amphlett, L.M. Kearns, R.F. Mann, Appl. Catal. A 179 (1999) 21.
[7] B.L. Kniep, F. Girgsdies, T. Ressler, J. Catal. 236 (2005) 34.
[8] A.A.G. Lima, M. Nele, E.L. Moreno, H.M.C. Andrade, Appl. Catal. A 171 (1998) 31.
[9] J.H. Schlander, T. Turek, Ind. Eng. Chem. Res. 38 (1999) 1264.
[10] V.Z. Fridman, A.A. Davydov, J. Catal. 195 (2000) 20.
[11] M. Saito, K. Murata, Catal. Surv. Asia 8 (2004) 285.
[12] T. Ressler, B.L. Kniep, I. Kasatkin, R. Schlogl, Angew. Chem. Int. Ed. 44 (2005) 4704.
[13] M.M. Gunter, T. Ressler, R.E. Jentoft, B. Bems, J. Catal. 203 (2001) 133.
[14] M.M. Gunter, T. Ressler, B. Bems, C. Buscher, T. Genger, O. Hinrichsen, M. Muhler, R. Schlogl, Catal. Lett. 71 (2001) 37.
[15] B.L. Kniep, T. Ressler, A. Rabis, F. Girgsdies, M. Baenitz, F. Steglich, R. Schlogl, Angew. Chem. Int. Ed. 43 (2004) 112.
[16] P.H. Matter, U.S. Ozkan, J. Catal. 234 (2005) 463.
[17] P.H. Matter, D.J. Braden, U.S. Ozkan, J. Catal. 223 (2004) 340.
[18] X.R. Zhang, L.C. Wang, C.Z. Yao, Y. Cao, W.L. Dai, H.Y. He, K.N. Fan, Catal. Lett. 102 (2005) 183.
[19] L. Alejo, R. Lago, M.A. Pena, J.L.G. Fierro, Appl. Catal. A 162 (1997) 281.
[20] J.P. Breen, J.R.H. Ross, Catal. Today 51 (1999) 521.
[21] J.L. Li, T. Inui, Appl. Catal. A 137 (1996) 105.
[22] H.G. El-Shobaky, M. Mokhtar, G.A. El-Shobaky, Appl. Catal. A 180 (1999) 335.
[23] C.L. Carnes, K.J. Klabunde, J. Mol. Catal. A 194 (2003) 227.
[24] J. Agrell, M. Boutonnet, I. Melian-Cabrera, J.L.G. Fierro, Appl. Catal. A 253 (2003) 201.
[25] J. Agrell, M. Boutonnet, J.L.G. Fierro, Appl. Catal. A 253 (2003) 213.
[26] L. Huang, G.J. Kramer, W. Wieldraaijer, D.S. Brands, E.K. Poels, H.L. Castricum, H. Bakker, Catal. Lett. 48 (1997) 55.
[27] H.L. Castricum, H. Bakker, B. van der Linden, E.K. Poels, J. Phys. Chem. B 105 (2001) 7928.
[28] H.L. Castricum, H. Bakker, E.K. Poels, Mater. Sci. Eng. A 304–306 (2001) 418.
[29] R. Becker, H. Parala, F. Hipler, O.P. Tkachenko, K.V. Klementiev, W. Grunert, H. Wilmer, O. Hinrichsen, A. Birkner, M. Muhler, C. Woll, S. Schafer, R.A. Fisher, Angew. Chem. Int. Ed. 43 (2004) 2839.
[30] J.R. Jensen, T. Johannessen, S. Wedel, H. Livbjerg, J. Catal. 218 (2003) 67.
[31] Y. Choi, H.G. Stenger, Appl. Catal. B 38 (2002) 259.
[32] W. Cheng, Acc. Chem. Res. 32 (1999) 685.
[33] J.F. Deng, Q. Sun, Y.L. Zhang, S.Y. Chen, D. Wu, Appl. Catal. A 139 (1996) 75.
[34] Y.A. Skakov, Met. Sci. Heat Treat. 47 (2005) 296.
[35] S. Kaliaguine, A. Van Neste, V. Szabo, J.E. Gallot, M. Bassir, R. Muzychuk, Appl. Catal. A 209 (2001) 345.
[36] D.A. Bulushev, L. Kiwi-Minsker, V.I. Zaikovskii, A. Renken, J. Catal. 193 (2000) 145.
[37] V.V. Boldyrev, K. Tkacova, J. Mater. Synth. Process. 8 (2000) 121.
[38] A. Trovarelli, F. Zamar, J. Llorca, C. deLeitenburg, G. Dolcetti, J.T. Kiss, J. Catal. 169 (1997) 490.
[39] V.V. Molchanov, R.A. Buyanov, Kinet. Catal. 42 (2001) 366.
[40] X.R. Zhang, L.C. Wang, Y. Cao, W.L. Dai, H.Y. He, K.N. Fan, Chem. Commun. (2005) 4104.
[41] Y.M. Liu, W.L. Feng, T.C. Li, H.Y. He, W.L. Dai, W. Huang, Y. Cao, K.N. Fan, J. Catal. 239 (2006) 125.
[42] G.C. Chinchen, C.M. Hay, H.D. Vandervell, K.C. Waugh, J. Catal. 103 (1987) 79.
[43] M.A. Gabala, S.S. Ata-Allah, J. Phys. Chem. Solids 65 (2004) 995.
[44] J. Perez-Ramirez, G. Mul, J.A. Moulijn, Vib. Spectrosc. 27 (2001) 75.
[45] M.A. Gabal, Thermochim. Acta 402 (2003) 199.
[46] W.L. Dai, Q. Sun, J.F. Deng, D. Wu, Y.H. Sun, Appl. Surf. Sci. 177 (2001) 172.
[47] J. Agrell, H. Birgersson, M. Boutonnet, I. Melian-Cabrera, R.M. Navarro, J.L.G. Fierro, J. Catal. 219 (2003) 389.
[48] T. Schedel-Niedrig, M. Hävecker, A. Knop-Gericke, R. Schlögl, Phys. Chem. Chem. Phys. 2 (2000) 3473.
[49] A. Knop-Gericke, M. Hävecker, T. Schedel-Niedrig, R. Schlögl, Top. Catal. 15 (2001) 27.
[50] T.L. Reitz, S. Ahmed, M. Krumpelt, R. Kumar, H.H. Kung, J. Mol. Catal. A 162 (2000) 275.
[51] F. Raimondi, K. Geissler, J. Wambach, A. Wokaun, Appl. Surf. Sci. 189 (2002) 59.
[52] O. Yasuakl, F. Klyotaka, I. Toshlnobu, T. Shllchlro, J. Phys. Chem. 87 (1983) 3747.
[53] E.B. Batyrev, J.C. van den Heuvel, J. Beckers, W.P.A. Jansen, H.L. Castricum, J. Catal. 229 (2005) 136.
[54] S. Indris, R. Amade, P. Heitjans, M. Finger, A. Haeger, D. Hesse, W. Grulnert, A. Bolrger, K.D. Becker, J. Phys. Chem. B 109 (2005) 23,274.
[55] R. Zhang, A. Villanueva, H. Alamdari, S. Kaliaguine, Appl. Catal. B Environ. 64 (2006) 220.
[56] T.E. Davies, T. Garcı´a, B. Solsona, S.H. Taylor, Chem. Commun. (2006) 3417.
[57] V.D. Kumari, M. Subrahmanyam, A. Ratnamala, D. Venugopal, B. Srinivas, M.V.P. Sharma, S.S. Madhavendra, B. Bikshapathi, K. Venkateswarlu, T. Krishnudu, K.B.S. Prasad, K.V. Raghavan, Catal. Commun. 3 (2002) 417.
[58] M. Kurtz, H. Wilmer, T. Genger, O. Hinrichsen, M. Muhler, Catal. Lett. 86 (2003) 77.